Acta Biomaterialia 123 (2021) 312–324

Contents lists available at ScienceDirect

Acta Biomaterialia

journal homepage: www.elsevier.com/locate/actbio

Full length article

Three-dimensional endothelial cell incorporation within bioactive nanofibrous scaffolds through concurrent emulsion electrospinning and coaxial cell electrospraying

Qilong Zhao [a,1,*], Yu Zhou [b,1], Min Wang [b,*]

[a] Institute of Biomedical & Health Engineering, Shenzhen Institutes of Advanced Technology, Chinese Academy of Sciences, Shenzhen 518035, China
[b] Department of Mechanical Engineering, The University of Hong Kong, Pokfulam Road, Hong Kong, China

ARTICLE INFO

Article history:
Received 3 September 2020
Revised 14 January 2021
Accepted 21 January 2021
Available online 27 January 2021

Keywords:
Concurrent manufacturing
3D cell incorporation
Tissue engineering
Electrospinning
Electrospraying
Vascularization

ABSTRACT

Nanofibrous scaffolds hold great promise in tissue engineering owing to their extracellular matrix (ECM)-mimicking architectures. Electrospinning, with its ease for producing nanofibrous scaffolds, has therefore been widely employed for various tissue engineering applications. However, electrospun nanofibrous scaffolds have faced the inherent challenge of three-dimensional (3D) cell distribution due to the small sizes of interconnected pores in these scaffolds when conventional approach of scaffold fabrication with subsequent cell seeding is adopted, which severely limits their applications in repairing/regenerating human body tissues with thick and vascularized structures. In this study, we demonstrate a method to directly place living endothelial cells within bioactive nanofibrous scaffolds in 3D through concurrent emulsion electrospinning and coaxial cell electrospraying. Using this concurrent manufacturing method, endothelial cells are encapsulated in hydrogel microspheres and deposited along with vascular endothelial growth factor (VEGF)-containing nanofibers in the scaffold fabrication process, resulting in nanofibrous scaffolds with 3D embedded cell-encapsulated microspheres. After selective disruption of the hydrogel microspheres, the encapsulated endothelial cells are released, yielding bioactive nanofibrous scaffolds with tissue-like 3D cell-incorporated nanofibrous structures. It is shown that cell viability is well preserved (>98%) during the concurrent manufacturing process and that a deep cell distribution (~100 μm) through the scaffold thickness has been achieved. With combined structural and biochemical cues via the 3D cell-incorporated architectures, endothelial cells can freely stretch, display enhanced intercellular connections, and maintain the phenotype in the bioactive nanofibrous scaffolds. Our investigations offer a promising platform technology for creating bioactive nanofibrous scaffolds with 3D cell incorporation and for overcoming inherent problems of electrospun nanofibrous scaffolds, which should open new avenues for biomanufacturing tissue-mimicking constructs with vascularized structures and complex anatomy.

Statement of significance

Electrospun nanofibrous scaffolds face challenges in three-dimensional (3D) cell incorporation and vascularization. Enhancing cell penetration via enlarged interconnected pores is a common strategy to address that. However, there are conflicts between cell penetration and structural integrity for scaffolds formed using such strategy, as deep cell penetration, if possible, can only achieve in highly loose architectures. In this investigation, we demonstrate a concurrent emulsion electrospinning and coaxial cell electrospraying technique, realizing 3D endothelial cell incorporation in electrospun nanofibrous scaffolds independent of cell penetration. Our technology appropriately addresses the conflict between deep 3D cell incorporation and structural

* Corresponding authors.
E-mail addresses: ql.zhao@siat.ac.cn (Q. Zhao), memwang@hku.hk (M. Wang).
[1] These authors contributed equally to this work.

https://doi.org/10.1016/j.actbio.2021.01.035
1742-7061/© 2021 Acta Materialia Inc. Published by Elsevier Ltd. All rights reserved.

integrity. In the scaffolds, the 3D incorporated endothelial cells show well-preserved viability, phenotype and functions, implying improved vascularization potential.

© 2021 Acta Materialia Inc. Published by Elsevier Ltd. All rights reserved.

1. Introduction

With the aim of regenerating body tissues effectively, biomedical materials should be not only bioresorbable but also bioactive in order to support cell ingrowth, direct cell behaviors, and assist to form regenerated or reconstituted tissues [1]. In nature, extracellular matrix (ECM) plays vital roles in supporting cell ingrowth and directing cell behaviors in three-dimensions (3D) by offering on-demand structural, mechanical and biological cues [2]. Tissue engineering scaffolds, as artificial extracellular microenvironments for providing the functions of ECM [3–5], should therefore mimic the nanofibrous architectures and bioactivities of ECM, as well as the natural 3D cell-ECM organizations. Electrospinning is a facile and versatile technique for producing nanofibers with desired compositions, adjustable mechanical properties and the incorporation of specific bioactive molecules, thereby holding great promise in fabricating scaffolds with ECM-resembling architectures, mechanics and bioactivities for various tissue engineering applications [6–8]. However, conventional electrospun nanofibrous scaffolds face inherent problems of two-dimensional (2D) cell incorporation and limited cell infiltration that is restricted by the small sizes of interconnected pores [9], which highly affect cell ingrowth and vascularization when they are used to repair thick body tissues or solid organs. To address these challenges, many efforts, such as sacrificial strategy and microfiber-nanofiber co-deposition strategy [10–15], have been made for enlarging the pore sizes of electrospun scaffolds and hence enhancing cell penetration into the scaffolds. However, with these strategies, the ECM-mimicking nanofibrous architectures and the structural integrity of the electrospun scaffolds with enlarged pores may be damaged. Therefore, new strategies should be investigated and developed to achieve 3D cell incorporation within electrospun nanofibrous scaffolds without significantly compromising ECM-mimicking nanofibrous architectures and structural integrity.

Through seeding cells within electrospinning process in either an alternate or a sequential manner [16,17], cells could be directly placed in the nanofibrous architectures of the electrospun scaffolds. However, both the lack of necessary protection on the seeded cells and the evaporation of organic solvents during the electrospinning process affect cell viability. In recent years, microfluidics-assisting coaxial cell electrospraying attracts increasing attentions in the fields of cell microencapsulation and cell delivery and cell protection [18,19]. In addition, coaxial cell electrospraying is readily to be integrated with electrospinning, bringing up the possibility of effectively incorporating living cells within nanofibrous scaffolds via a new concurrent manufacturing process. In this study, we investigate the creation of nanofibrous scaffolds with 3D endothelial cell incorporation through concurrent electrospinning and coaxial cell electrospraying (Fig. 1). In the proof-of-concept study, human umbilical vascular endothelial cells (HUVECs) are placed within the vascular endothelial growth factor (VEGF)-containing emulsion electrospun poly(lactic-*co*-glycolic acid) (PLGA) nanofibrous scaffolds via coaxial electrosprayed calcium-ion-crosslinked alginate (Ca-alginate) hydrogel microspheres. Due to the excellent cytocompatibility and mild condition of cross-linking [19], Ca-alginate hydrogel microspheres have been proven to a desirable vehicle for encapsulating and protecting cells to be delivered. Also, VEGF-releasing PLGA scaffolds are shown to be good structural platforms owing to their appropriate mechanical properties, biodegradability and bioactivities for supporting the attachment and growth of endothelial cells [20,21]. Through our new concurrent manufacturing process, tissue-like 3D cell incorporation within the bioactive nanofibrous extracellular microenvironments has been successfully realized. Very importantly, the resulting 3D cell-incorporated nanofibrous scaffolds exhibit well-preserved structural integrity and possess comparable mechanical properties to native soft tissues. With the assistance of the biomimetic architectures, mechanical properties and 3D cell-nanofiber organizations, as well as enhanced bioactivities endowed by the sustained release of VEGF, the endothelial cells in the nanofibrous scaffolds can form intercellular connections, which indicates the potential of improved 3D vascularization. Furthermore, as a platform technology for creating bioactive nanofibrous 3D cell-incorporated constructs, concurrent emulsion electrospinning and coaxial cell electrospraying is highly promising for engineering tissue substitutes with complicate anatomy and 3D multicellular structures.

2. Materials and methods

2.1. Materials

Medical grade PLGA with a LA:GA molar ratio of 50:50 (average Mw=120,000) was purchased from Lakeshore Biomaterials (USA). Deionized water (DI water) was produced by a DI water producer (Model D12681, Barnstead International, USA). Sodium alginate (Na-alginate), calcium chloride ($CaCl_2$), sodium citrate (Na-citrate), trifluoroethanol (TFE), sodium azide, bovine serum albumin (BSA), Tween-20, tablets for preparing phosphate buffer saline (PBS), and a H_2O_2-sensitive fluorophore, dichlorofluorescein diacetate (DCFDA), for probing the intracellular reactive oxygen species (ROS) level were products of Sigma-Aldrich (USA). VEGF (Recombinant Human $VEGF_{165}$) and the corresponding enzyme-linked immunosorbent assay (ELISA) kit (Human $VEGF_{165}$ Standard ABTS ELISA Development Kit) were products of PeproTech Inc. (USA). A LIVE/DEAD viability kit for evaluating cell viability was purchased from Invitrogen (UK), with which live cells would be stained by calcein acetoxymethylester (Calcein-AM) to green and dead cells would be stained by ethidium homodimer-1 (EthD-1) to red. Alexa Fluor 488 Phalloidin, 4′,6-diamidino-2-phenylindole (DAPI), a mouse monoclonal anti-CD31 antibody, and an Alexa Fluor 568 goat anti-mouse secondary antibody for staining actin filaments (F-actin), nucleus and CD31 of HUVECs, respectively, were purchased from Abcam (USA).

2.2. Cell culture

A human primary endothelial cell, HUVEC, was used in the experiments, which was purchased from Life Technologies (USA) and cultured in an endothelial-specific cell culture medium, medium 200 (M200, Life Technologies, USA), with supplemented 2% v/v low serum growth supplement (Life Technologies, USA), 100 units/mL penicillin-streptomycin (Life Technologies, USA), and 4 μg/mL fungizone (Life Technologies, USA). The cultured HUVECs were maintained in a 37°C, 5% CO_2, humidified cell culture incubator (Thermo Fisher Scientific, USA). At passage 2 and 3 with 70% cell confluence, HUVECs were trypsinized to cell suspensions for coaxial cell electrospraying or cell seeding experiments. All materials used in the

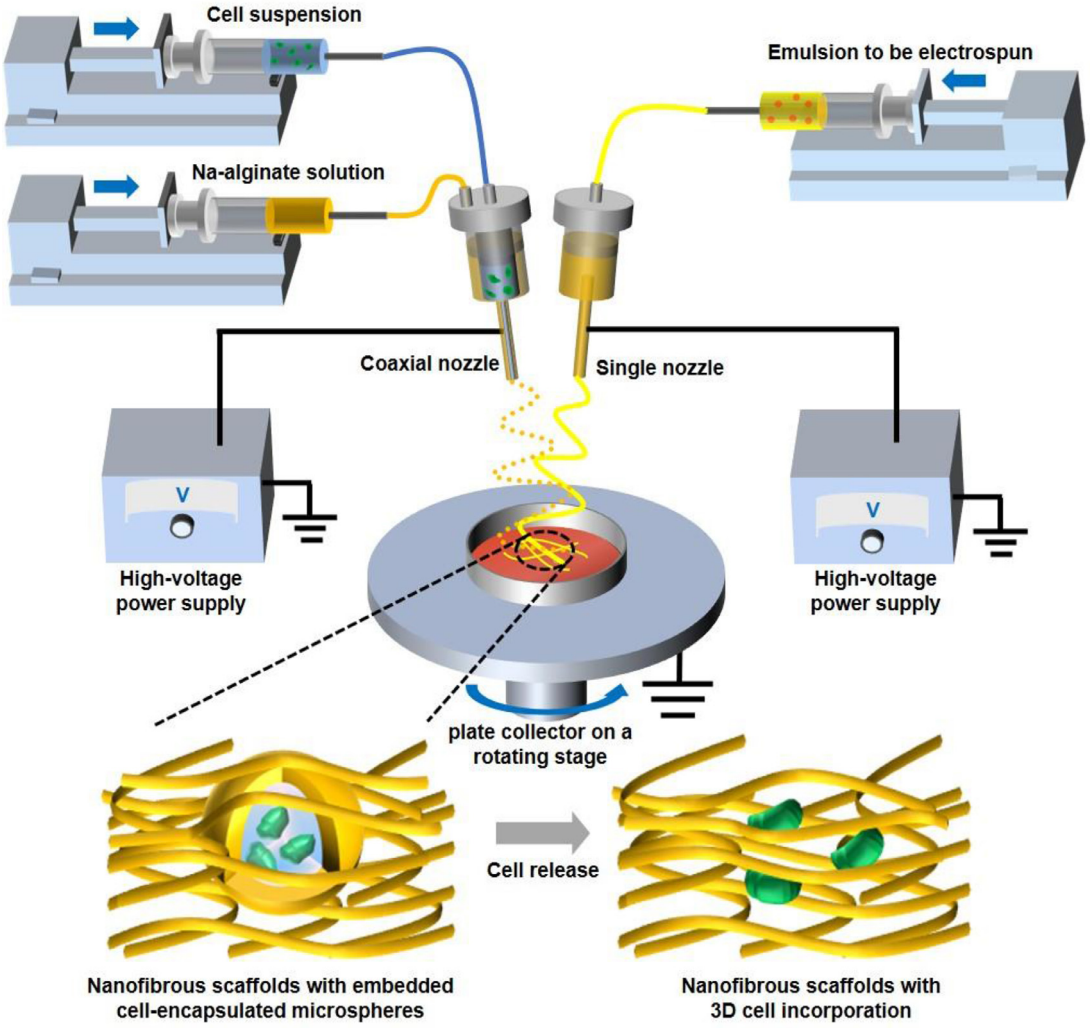

Fig. 1. A schematic diagram showing the concurrent emulsion electrospinning and coaxial cell electrospraying process for fabricating firstly nanofibrous scaffolds embedded with cell-encapsulated microspheres and subsequently nanofibrous scaffolds with 3D cell incorporation after the release of encapsulated cells from microspheres.

cell culture and coaxial cell electrospraying experiments were presterilized under a gamma radiation from Cobalt 60 sources with an intensity of 15 kGy for 30 minutes. And the cell culture and coaxial cell electrospraying experiments were performed in a Class II, type A laminar flow culture hood (Thermo Fisher Scientific, USA).

2.3. Coaxial cell electrospraying

During coaxial cell electrospraying, a coaxial nozzle was used [22], where the compound jetting containing one Na-alginate solution outer phase and one inner phase (PBS or cell suspension) from the coaxial nozzle was sprayed towards a $CaCl_2$ aqueous solution (1.5% w/v) and subsequently crosslinked to form Ca-alginate hydrogel microspheres. For determining the appropriate processing parameters for coaxial cell electrospraying, cell-free coaxial electrospraying using PBS as the inner phase was firstly investigated. The processing parameters (i.e., feeding rates for the out phase and inner phase and the applied voltage) in coaxial electrospraying were varied (Table 1), resulting in Ca-alginate hydrogel microspheres with diverse structures (designated as CES1 to CES5, correspondingly). The structures of Ca-alginate microspheres formed under different conditions were studied using a fluorescence microscope (Eclipse TE2000-U inverted microscope, Nikon, Japan) in the bright field mode. The diameters of Ca-alginate microspheres formed under different conditions were measured by using the software Image J, and their average diameters were statistically analyzed ($N > 50$).

Table 1
Processing parameters for fabricating Ca-alginate hydrogel microspheres through coaxial electrospraying.

	Feeding rate (mL/h)		Applied voltage (kV)
	Na-alginate (4% w/v)	PBS	
CES1	2.0	1.0	8.0
CES2	2.0	1.0	12.0
CES3	2.0	1.0	16.0
CES4	2.0	1.5	16.0
CES5	2.0	2.0	16.0

Using appropriate processing parameters determined from the cell-free coaxial cell electrospraying experiments, coaxial cell electrospraying using cell suspensions having different densities of HUVECs (1×10^7 and 5×10^6 cells/mL, corresponding to the high and low cell density conditions, respectively) as the inner phase was then performed. A collection bath filled with M200 with the addition of $CaCl_2$ (1.5% w/v) was placed under the coaxial nozzle for collecting cell-encapsulated Ca-alginate hydrogel microspheres. The morphologies and structures of the cell-encapsulated Ca-alginate hydrogel microspheres were studied using bright-field

microscopy. The viability and the intracellular ROS level of encapsulated cells in Ca-alginate microspheres formed at the low and high cell density were characterized by staining the cells with the LIVE/DEAD viability staining kit and DCFDA, respectively, which were observed under the fluorescence microscope. The average diameter, cell viability, percentage of cells with high intracellular ROS levels (calculated according to the amounts DCFDA probing cells with respect to the total number of cells in one microsphere), and number of cells per microsphere for the cell-encapsulated microspheres were analyzed ($N > 50$).

To release the encapsulated cells on demand, cell release treatments by dripping a dilute Na-citrate aqueous solution (0.055 M) on cell-encapsulated Ca-alginate hydrogel microspheres were performed. After dripping the Na-citrate solution, the structural changes of the microspheres over time were recorded under bright-field microscopy. The intracellular ROS levels of released cells after 12-h cell culture were characterized by staining the cells with DAPI and DCFDA according to the manufacturer' protocol and observed under the fluorescence microscope, where the manually seeded the cells were stained and observed using the same procedures as control. The mean intensity of DCFDA per cell for the released cells and the control was separately analyzed using the software ImageJ by calculating the mean intensity of DCFDA with respect to the total number of cells in one picture ($N = 3$). The released cells were then incubated. The viability and the density of the cells immediately after release (Day 0) and after culture for different time periods (Day 1, 3 and 7) were investigated through staining the cells using the LIVE/DEAD viability staining kit, observing and imaging them under the fluorescence microscope and conducting analysis of the images using ImageJ ($N = 3$).

2.4. Concurrent emulsion electrospinning and coaxial cell electrospraying

Concurrent emulsion electrospinning and coaxial cell electrospray, as illustrated in Fig. 1, was performed to fabricate firstly VEGF-containing emulsion electrospun PLGA scaffolds with embedded cell-encapsulated Ca-alginate microspheres (i.e., "microsphere-embedded scaffolds"). The bioactive nanofibrous PLGA scaffolds with 3D incorporation of endothelial cells (i.e., "3D cell-incorporated scaffolds") were made from microsphere-embedded scaffolds after selective disruption of the Ca-alginate microspheres by the cell release treatment. Emulsion electrospinning was conducted according to the established method [21]. In brief, an emulsion was prepared by mixing a PLGA solution (20% w/v in TFE) and a VEGF-containing PBS (10 mg/mL) at a volume ratio of 10:1 under vigorous mechanical stirring, which was then electrospun at a static electric field (15 kV) generated by a negative high-voltage power supply to obtain VEGF-incorporated emulsion electrospun PLGA scaffolds (i.e., normal emulsion electrospun PLGA scaffolds). During concurrent emulsion electrospinning and coaxial electrospraying, VEGF-incorporated PLGA nanofibers and cell-encapsulated Ca-alginate microspheres were simultaneously deposited into a plate collector filled with the M200 medium having 1.5% w/v $CaCl_2$ and placed on a grounded rotating stage. For samples in comparative studies, concurrent emulsion electrospinning and coaxial electrospraying using a VEGF-free emulsion was also conducted, resulting in VEGF-free and 3D cell-incorporated scaffolds as the control.

2.5. Morphological, structural and mechanical characterization and in vitro degradation study

The morphologies and structures of the scaffolds formed by concurrent emulsion electrospinning and coaxial cell electrospray (before and after the cell release treatment) were studied using a field emission scanning electron microscope (SEM, LEO 1530, Germany). Samples for SEM observations were freeze-dried for 48 hours and then sputter-coated (50 seconds) with a thin layer of gold. The scaffolds formed by the concurrent manufacturing process and cell release treatment were characterized by using a Fourier transform infrared (FTIR) spectrometer (IRAffinity-1S, Shimadzu, Japan), while normal electrospun PLGA scaffolds and electrosprayed Ca-alginate microspheres were used as controls. The meso-structures of emulsion electrospun PLGA fibers were characterized by using a transmission electron microscope (TEM, Philips CM100, the Netherlands). The mechanical properties (including elastic modulus, ultimate tensile strength and fracture strain) of normal PLGA scaffolds, microsphere-embedded scaffolds and 3D cell-incorporated scaffolds were determined according to their strain-stress curves ($N = 6$) obtained through tensile tests, which were performed on a tabletop Instron tester (Model 5848) following the American Society for Testing Materials test standard (ASTM C1557). The *in vitro* degradation properties of the normal electrospun PLGA scaffolds and microsphere-embedded scaffolds were also evaluated through the immersion treatment according to the established procedures [6]. Pre-weighed scaffolds were immersed in individual bottles filled with PBS with supplemented 0.02% w/v sodium azide (for the antibacterial purpose) and placed in a shaking water bath at 37°C, with the immersion medium being refreshed every 2 days. At different time points of immersion (1, 2, 3 and 4 weeks), they were taken out, washed with DI water, dried and weighed. The weight loss (in percentages) over immersion time for the scaffolds were plotted ($N = 3$) and the morphologies of PLGA scaffolds before immersion and after 3-week immersion were observed under the SEM.

2.6. In vitro VEGF release experiments

The total contents of VEGF incorporated in emulsion electrospun PLGA scaffolds were calculated according to the ELISA measurements on the extraction solutions after completely dissolving pre-weighed scaffolds and the reference curve for VEGF concentration measurements was established by using VEGF standard solutions. After immersing pre-weighed normal emulsion electrospun PLGA scaffolds in the medium of PBS supplemented with 0.02% w/v sodium azide (for the antibacterial purpose), 0.05% v/v Tween-20 (for reducing nonspecific protein absorption) and 0.5% w/v BSA (for stabilizing released VEGF), the immersion medium were collected at preset time points and the contents of VEGF in the immersion medium were measured through ELISA, using a microplate reader (UVM 340, Asys HiTech GmbH, Australia) at a measuring wavelength of 405 nm with a reference wavelength of 650 nm. The *in vitro* release profile for VEGF was established by plotting cumulative release percentages of the released VEGF with respect to the total VEGF content against immersion time ($N = 3$).

2.7. Endothelial cell distribution, morphology, cytoskeleton development and phenotypic assessments

To assess the viability of cells put in scaffolds fabricated by the concurrent manufacturing process, cells in microsphere-embedded scaffolds and in 3D cell-incorporated scaffolds were stained by using the LIVE/DEAD viability kit and then examined under the fluorescence microscope immediately after scaffold manufacture. Also, after 1-day cell culture, the distribution of cells in the 3D cell-incorporated scaffolds was studied, where the cells were stained by Calcein-AM and the 3D cell-incorporated scaffolds were subsequently observed under a laser scanning confocal microscope (LSCM, LSM710, Carl Zeiss, Germany). Furthermore, 3D cell-incorporated scaffolds after 1-day cell culture were fixed by using 4% v/v paraformaldehyde, treated with a series of ethanol solutions

of increasing ethanol concentrations, free-dried for 48 h, and observed under the SEM for studying the cell morphology. To investigate the cytoskeleton development and phenotype of cells within 3D cell-incorporated scaffolds, HUVECs were seeded onto emulsion electrospun VEGF-containing PLGA scaffolds (i.e., "VEGF-releasing 2D cell-incorporated scaffolds") through post-electrospinning manual cell seeding or incorporated into emulsion electrospun VEGF-free PLGA scaffolds (i.e., "VEGF-free 3D cell-incorporated scaffolds") and emulsion electrospun VEGF-containing PLGA scaffolds (i.e., "VEGF-releasing 3D cell-incorporated scaffolds") made by our new concurrent manufacturing process. After 3-day cell culture, the cytoskeleton development of cells grown on/in the three types of scaffolds was studied by staining the cells with Alexa Fluor 488 Phalloidin and DAPI according to the manufacturer's protocol. After 5-day cell culture, the phenotype of cells grown on/in different scaffolds was studied by staining the cells with mouse monoclonal anti-CD31 antibody, Alexa Fluor 568 goat anti-mouse secondary antibody, Alexa Fluor 488, Phalloidin and DAPI according to the manufacturer's protocol.

2.8. Statistical analysis

The results of numerical values obtained in this study were expressed as mean ± standard deviation (SD). For results obtained from different conditions or groups, statistical analyses were conducted using Analysis of Variance (ANOVA) with Student's t-test. Non-significant (n. s.) in the analyses states that there was no statistically significant difference. $P < 0.05$ (*) and $P < 0.01$ (**) were considered as statistically significant.

3. Results

3.1. Endothelial cell encapsulation through coaxial cell electrospraying and on-demand release of encapsulated cells

Effectively placing living cells with sufficient protection for the cells is highly important for successfully creating clinically usable 3D cell-incorporated scaffolds. In our investigations, coaxial cell electrospraying, which can be readily integrated with electrospinning, has been employed and studied for fabricating Ca-alginate hydrogel microspheres for cell delivery. To prepare Ca-alginate microspheres with appropriate diameters and well-preserved cell viability via coaxial cell electrospraying, processing parameters, including applied voltage and feeding rates, that may affect the microsphere structure and cell viability were therefore studied and tuned. The influences of applied voltage on the formation of Ca-alginate microspheres (CES1 to CES3 conditions, Table 1) were firstly investigated through cell-free coaxial electrospraying. To minimize the potential damages of electrostatic stretch on encapsulated cells, a low applied voltage would be preferred [23]. However, a too low voltage may be inadequate to generate stable Taylor cone during coaxial electrospraying for yielding uniform spherical microspheres [24]. When changing the applied voltage in coaxial electrospraying, three different jetting modes, i.e., dripping mode, transition mode (coning mode), and stable cone-jet mode, can be exhibited, which correspond to the formation of irregular shape microspheres with very large diameters of ~1000 μm (Fig. S1a), spherical shape microspheres with still large diameters of ~1000 μm (Fig. S1b), and uniform spherical shape microspheres with small diameters of ~100 μm (Fig. S1c), respectively. In addition, the influences of feeding rates of the inner phase and outer phase in the coaxial spinneret on the structures of electrosprayed microspheres were also studied. With an increase in the feeding rate ratio for the inner phase and outer phase, the diameter of electrosprayed microspheres increased and the intactness of microspheres was reduced accordingly (Figs. S1c to S1f) because the increased conductivity and reduced viscosity of the compound jetting could enhance the instability of electrospraying [25]. The results obtained in our investigation showed that microspheres prepared at the applied voltage of 16 kV and the feeding rate ratio of 1.0 or 2.0 for the inner phase and outer phase (the CES 3 condition) would be suitable for the cell delivery purpose and subsequently making cell-incorporated scaffolds owing to not only their uniform spherical shape but also their small diameters that should facilitate the dispersion of cell-encapsulated microspheres within the nanofibrous structures of electrospun scaffolds with minimal influences on the structural integrity of scaffolds.

Employing the CES 3 processing parameters, coaxial cell electrospraying was subsequently conducted using cell suspensions of different HUVEC densities (1×10^7 and 5×10^6 cells/mL, designated as high and low cell density condition, respectively). Both types of cell-encapsulated Ca-alginate microspheres with high or low cell density exhibited similar uniform spherical shapes with random distribution of encapsulated cells inside the microspheres (Figs. 2A and 2B). The average diameter of microspheres formed for the low cell density was slightly larger than those formed for the high cell density (Fig. 2C). To assess the influence of the coaxial cell electrospraying process on cell viability, the encapsulated cells in the microspheres formed at the low and high cell densities were stained by using the LIVE/DEAD viability kit (Fig. 2A and 2B) and the intracellular ROS levels were probed by using the H_2O_2-sensitive fluorophore, DCFDA (Fig. 2D and 2E). The encapsulated cells showed very high cell viability (>98%) in both types of cell-encapsulated Ca-alginate microspheres (Fig. 2F) and the percentages of encapsulated cells with a high intercellular ROS level were below 10% for these microspheres (Fig. 2G). There were no statistically significant differences in the cell viability and the percentage of cells with high intercellular ROS level between the two types of microspheres (Fig. 2F and 2G), revealing that the cell viability was well maintained in the Ca-alginate microspheres fabricated via coaxial cell electrospraying for both low and high cell densities.

To compare cell encapsulation for microspheres with low and high cell densities, the average number of encapsulated cells per microsphere ($\boldsymbol{N_{avg}}$) and cell encapsulation capability ($\boldsymbol{E}$) were determined. $\boldsymbol{E}$ was calculated according to the following equation:

$$E = N_{avg}/V_{avg} = 6N_{avg}/\pi\varphi^3 \quad (1)$$

where $\boldsymbol{V_{avg}}$ and $\boldsymbol{\varphi}$ are the average volume and average diameter, respectively, of microspheres. Although the average number of encapsulated cells per microsphere formed for the high cell density was higher than that of microspheres formed for the low cell density (Fig. 2H), the cell encapsulation capability for microspheres formed for the high cell density was lower than that of microspheres formed for the low cell density (Fig. 2I) owing to the smaller average diameter of microspheres formed for the lower cell density. Overall, coaxial cell electrospraying using a cell suspension with a low cell density (5×10^6 cells/mL) had resulted in cell-encapsulated microspheres with well-preserved cell viability, smaller microsphere diameters and higher cell encapsulation capability, which would be used in the subsequent concurrent manufacturing process.

Since the stability (or, biodegradability) of cell-encapsulated Ca-alginate hydrogel microsphere is affected by the crosslinking of Na-alginate by calcium ions in $CaCl_2$ solutions, it is therefore feasible to control the breakdown of microsphere structures for releasing the encapsulated cells on demand through selectively extracting the calcium ions from Ca-alginate hydrogels. Due to strong affinity between calcium ions and citrate anions [26], Na-citrate was employed in the current study to extract calcium ions from Ca-alginate microspheres for breaking down microsphere structures. The structural changes of cell-encapsulated Ca-alginate microspheres over time after the dripping of a dilute Na-

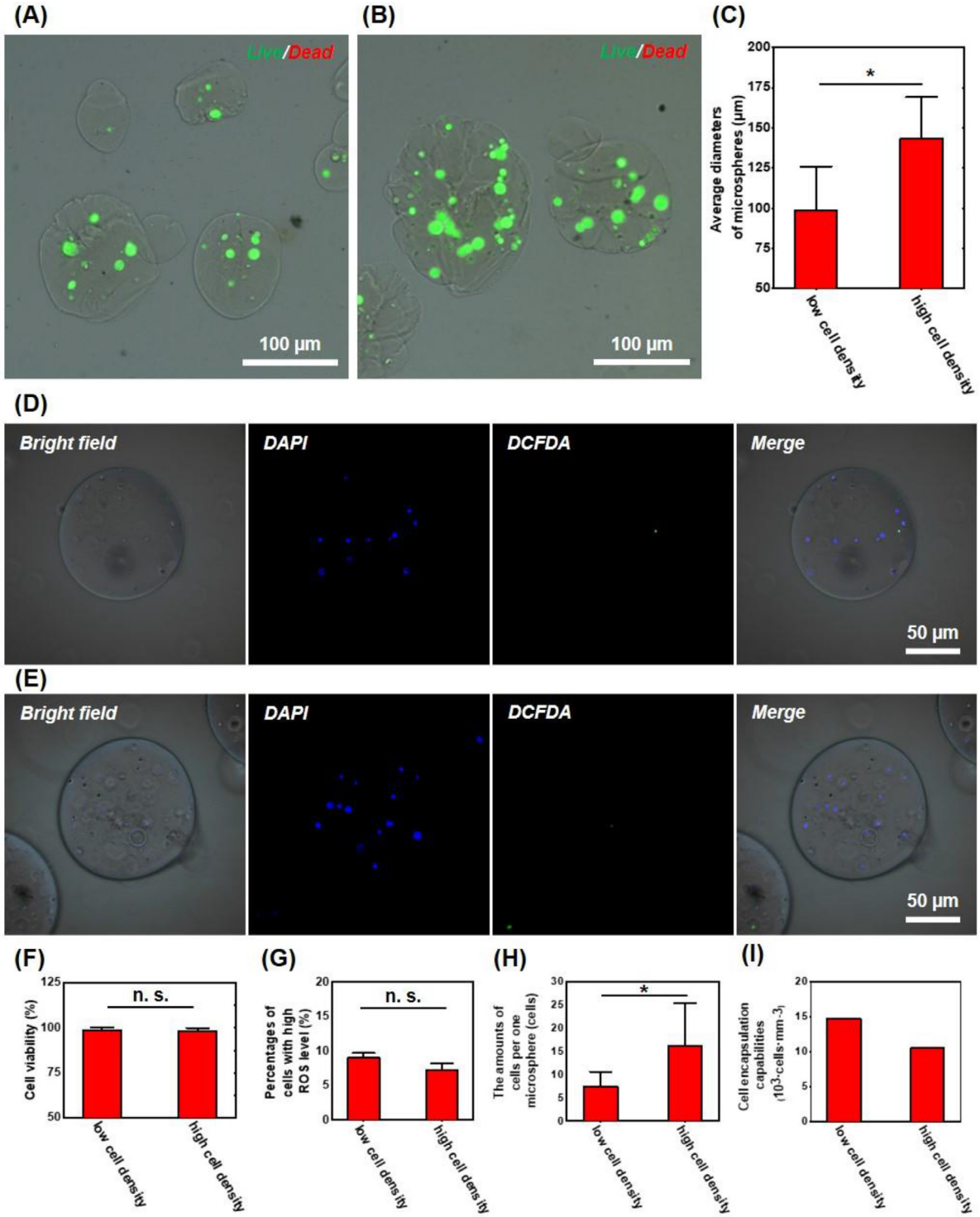

Fig. 2. Endothelial cell encapsulation in Ca-alginate hydrogel microspheres through coaxial cell electrospraying. (A) Cell-encapsulated Ca-alginate microspheres formed at the low cell density, with encapsulated cells being stained by using a LIVE/DEAD viability kit. (B) Cell-encapsulated Ca-alginate microspheres formed at the high cell density, with encapsulated cells being stained by using a LIVE/DEAD viability kit. (C) Average diameters of Ca-alginate microspheres formed for different cell densities. (D) Cell-encapsulated Ca-alginate microspheres formed for the low cell density, with encapsulated cells being stained by DAPI and DCFDA for labeling nucleus and probing intracellular ROS level, respectively. (E) Cell-encapsulated Ca-alginate microspheres formed for the high cell density, with encapsulated cells being stained by DAPI and DCFDA for labeling nucleus and probing intracellular ROS level, respectively. (F) Viability of encapsulated cells in Ca-alginate microspheres formed for different cell densities. (G) Percentage of cells with high intracellular levels in Ca-alginate microspheres formed for different cell densities. (H) Number of cells per cell-encapsulated Ca-alginate microsphere formed for different cell densities. (I) Cell encapsulation capability of Ca-alginate microspheres formed for different cell densities.

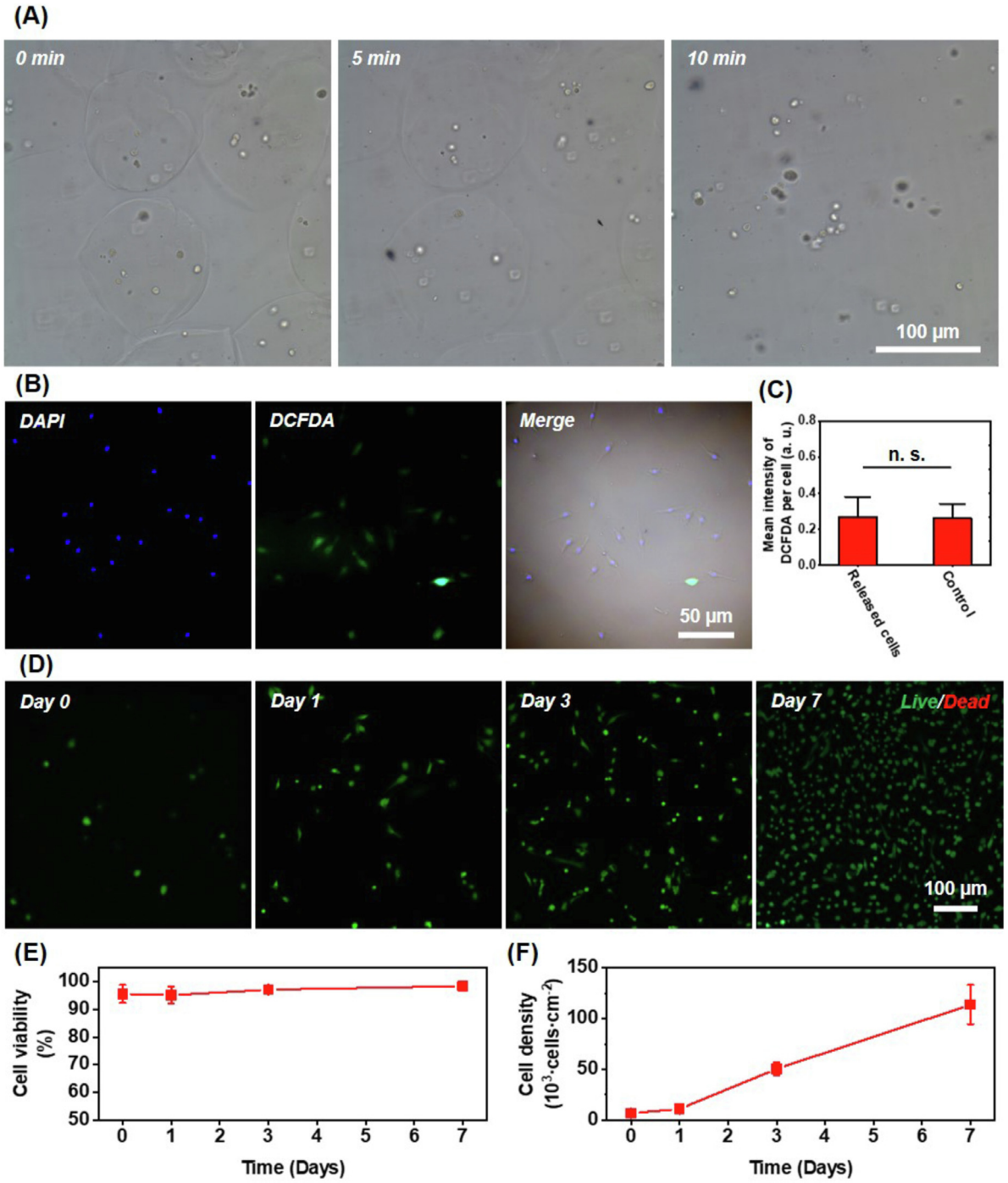

Fig. 3. On-demand release of endothelial cells from Ca-alginate microspheres and viability of released cells. (A) Structural changes over time for Ca-alginate microspheres after the cell release treatment. (B) Released endothelial cells stained by DAPI and DCFDA for labeling nucleus and probing intracellular ROS level, respectively, after 12 h of culture. (C) Analyses of the mean intensity of DCFDA per cell between the released cells and manually seeded cells (control) after 12 h of culture. (D) Released endothelial cells over culture time, with the cells being stained by using a LIVE/DEAD viability kit. (E) Analyses of the viability of the released cells after culturing for different time periods. (F) Analyses of the cell density of released cells after culturing for different times.

citrate aqueous solution (0.055M) on them were monitored *in situ* (Fig. 3A). It could be seen that after the Na-citrate solution treatment, the shapes of cell-encapsulated Ca-alginate microspheres changed from the original spherical shapes and were eventually disrupted, exhibiting obviously enlarged diameters after 5 mins. 10 mins later, the originally spherical structures of Ca-alginate microspheres could not be distinguished anymore and the encapsulated cells had been successfully released (Fig. 3A).

To assess the influence of cell release treatment on cell viability, the released cells were stained with DAPI (for revealing the amounts of cells), DCFDA (for probing intracellular ROS level), and the LIVE/DEAD viability kit (for labeling dead and live cells) af-

ter different cell culture times. After 12-h cell culture, endothelial cells were released from Ca-alginate microspheres; and after 12 h of culturing on a cell culture plate for cell attachment, endothelial cells showed similar intracellular ROS level as compared to the cells manually seeded on the cell culture plate (the control) under the same incubation condition (Fig. 3B **and** 3C **and Fig.** S2). There were no statistically significant differences in the intracellular ROS level between them (Fig. 3B), revealing that the endothelial cells that had undergone coaxial cell electrospraying and subsequent cell release treatment would not lead to enhanced apoptotic activities as compared to the cells directly seeded on scaffolds through manual procedures. In addition, the well-preserved cell viability of released cells was verified by the results of the LIVE/DEAD viability staining (Fig. 3D to 3F). Both the immediately released cells (Day 0) and cells after culture of 3, 5 and 7 days displayed high cell viability above 98% (Fig. 3E). The increases in cell numbers with the increase in culture time were also clearly observed (Fig. 3F), indicating the released cells could proliferate well. These results have shown the feasibility and effectiveness of coaxial cell electrospraying in cell microencapsulation and on-demand cell release with well-preserved cell viability, suggesting that it could be potentially applied for inputting living cells inside electrospun nanofibrous scaffolds.

3.2. Structural integrity, mechanical properties and bioactivity of scaffolds fabricated by concurrent emulsion electrospinning and coaxial cell electrospraying

Through integrating coaxial cell electrospraying with emulsion electrospinning to establish the concurrent manufacturing process, microsphere-embedded scaffolds were successfully made by the co-deposition of cell-encapsulated Ca-alginate microspheres and emulsion electrospun VEGF-containing PLGA fibers. The as-fabricated scaffolds exhibited nanofibrous structures with randomly arranged nanofibers (Fig. 4A), resembling the architectures of lyophilized natural ECM-derived scaffolds [27]. Microspheres with diameters ranging from several dozens of micrometers to one hundred micrometers were randomly distributed within the nanofibrous structures of scaffolds formed in the concurrent manufacturing process (Fig. 4A), indicating the successful 3D placements of Ca-alginate microspheres in the electrospun nanofibrous scaffolds by this fabrication technology. After the cell release treatment by dilute Na-citrate solution, the almost uniformly dispersed Ca-alginate microspheres disappeared from the scaffold structures (Fig. 4B), suggesting the selective disruption of the microsphere structures and hence the on-demand release of encapsulated cells. The FTIR results of the scaffolds indicated that embedded Ca-alginate microspheres could be completely broken down and eliminated from scaffolds by the cell release treatment as there was negligible characteristic absorption of Ca-alginate in FTIR spectra of Na-citrate treated scaffolds (Fig. S3). The overall nanofibrous architectures and the structural integrity were well maintained for 3D cell-incorporated scaffolds after the removal of Ca-alginate microspheres although some small voids were seen in the fibrous structures (Fig. 4B). The mechanical properties of microsphere-embedded scaffolds and 3D cell-incorporated scaffolds were investigated and compared with normal electrospun PLGA scaffolds (the control groups). Owing to the same composition in the matrix, i.e., the emulsion electrospun PLGA nanofibers, the three types of scaffolds showed similar elastic modulus according to their tensile stress-strain curves (Fig. S4). But due to the small differences in the structures among them (e.g., the small voids formed in 3D cell-incorporated scaffolds after cell release treatment), there were some differences in the ultimate tensile stress (Fig. 4C) and facture strain (Fig. 4D) for these three types of scaffolds. Despite some decreases in the ultimate tensile stress (~1 MPa) and facture strain (~30%) for 3D cell-incorporated scaffolds as compared to untreated scaffolds (Fig. 4C and 4D), their mechanical properties were still better or comparable to those of fibroblast-derived ECM as well as some soft tissues such as blood vessels [28], which would make them mechanically adequate for soft tissue engineering applications.

In 3D cell-incorporated scaffolds, a bioactive molecule, VEGF, was added for endowing the scaffolds with the bioactivity to enhance endothelial cell functions. The emulsion electrospun PLGA nanofibers were used as a vehicle for local VEGF delivery and the fibers showed core-shell meso-structures with aqueous cores (Fig. 4E). Within the aqueous cores of emulsion electrospun PLGA nanofibers, the bioactivity of VEGF could be well protected [21]. Along with molecular swelling and biodegradation of emulsion electrospun PLGA nanofibers in the *in vitro* tests (Fig. S5), VEGF could be released in a sustained and steady way (Fig. 4F), which could be employed to promote endothelial cell proliferation and spreading in the targeted spatiotemporal manner [29].

3.3. Endothelial cell viability, distribution, morphology, cytoskeleton development and phenotype in bioactive nanofibrous scaffolds

To investigate whether living endothelial cells could be incorporated within bioactive nanofibrous scaffolds in 3D through the concurrent manufacturing process, the viability of endothelial cells in the fabricated scaffolds was first evaluated by staining the cells using the LIVE/DEAD viability kit. From the fluorescence microscopic images and merged pictures (merging the bright-field and fluorescence channels), it was observed that endothelial cells with a high cell viability (>98%) were present inside Ca-alginate microspheres that were randomly distributed within the nanofibrous structures of microsphere-embedded scaffolds (Fig. 5A). After washing microsphere-embedded scaffolds with the culture medium for three times and subsequently releasing the encapsulated cells, the microspheres in the scaffolds disappeared, leaving randomly distributed cells within the nanofibrous structures of resultant scaffolds (Fig. 5B). Importantly, the released cells in the nanofibrous scaffolds also exhibited a high cell viability (>98%) (Fig. 5B). These results indicated that the Ca-alginate microsphere-based cell incorporation/cell delivery strategy did not harm the endothelial cells and could effectively protect them from potential damages of residual organic solvents in emulsion electrospun scaffolds. In addition, endothelial cells in the scaffolds after 1-day cell culture were labelled with Calcein-AM (for labelling living cells alone) and examined under a LSCM. It could be observed that living endothelial cells were located in the scaffolds with a deep cell distribution (~100 μm) through the scaffold thickness (Fig. 5C), which not only confirmed the successful 3D cell incorporation in scaffolds but also further proved the high viability preservation of endothelial cells incorporated in the scaffolds in 3D.

After ensuring that living endothelial cells could be successfully incorporated in bioactive nanofibrous scaffolds in 3D via our concurrent manufacturing process, the morphology, spreading, cytoskeleton developments, and phenotypes of the endothelial cells grown in the scaffolds were studied. For 3D cell-incorporated scaffolds after 1-day culture, cells with well-stretched morphologies could be clearly seen within the nanofibrous structures of scaffolds (Fig. 5D), exhibiting good cell spreading on nanofibers in scaffolds. Unlike the spreading of cells mainly on the surface of electrospun nanofibrous scaffolds for conventional electrospun scaffolds with subsequent manual cell seeding on their surfaces [30], the endothelial cells in scaffolds formed by our concurrent manufacturing technology existed inside the nanofibrous structures (Fig. 5D), which would result in more anchoring points for cells for better supporting 3D cell attachment that is more like the natural cell-ECM organization [31]. To assess whether the functions

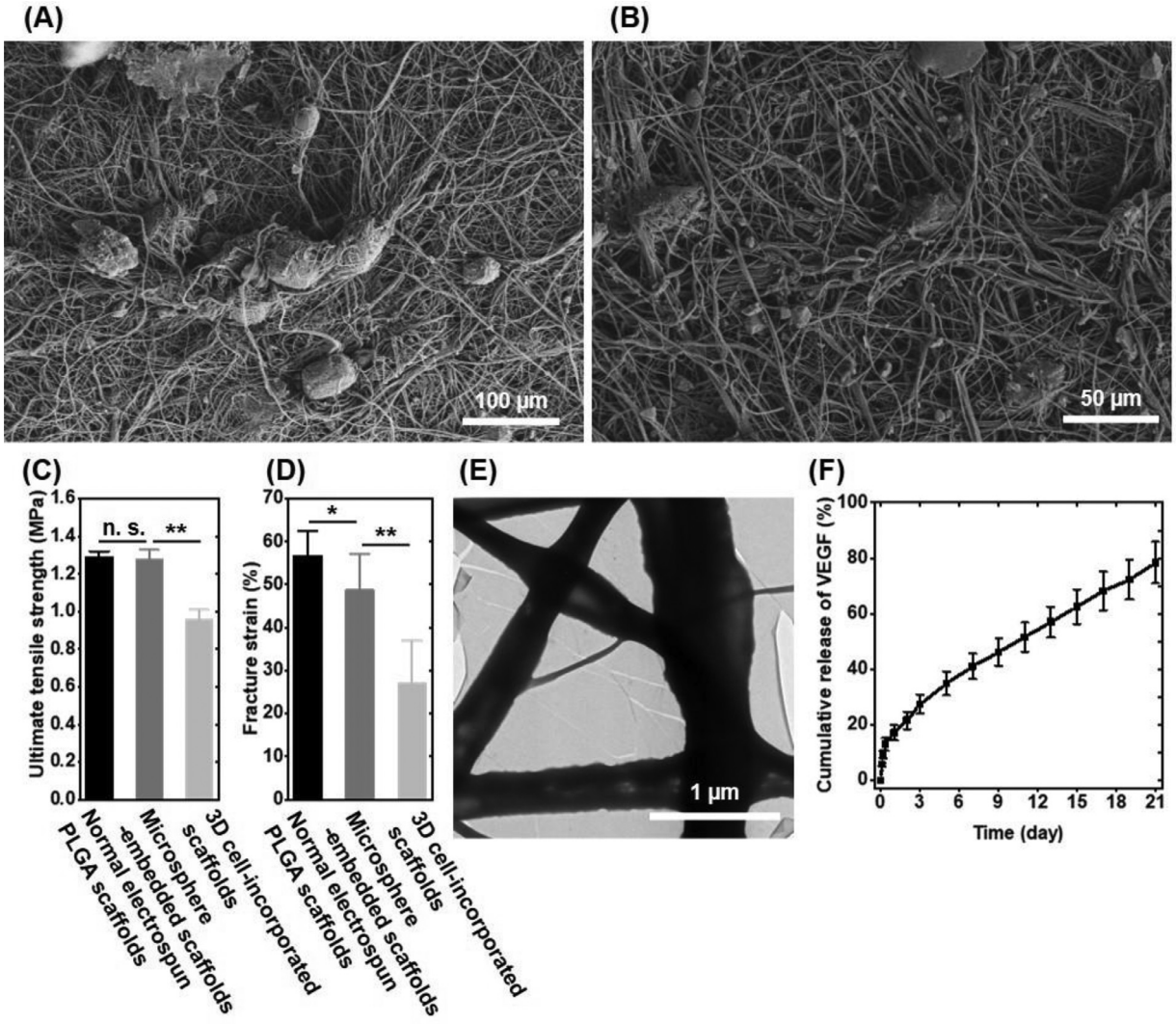

Fig. 4. Morphology, structure, mechanical properties and VEGF release profile of scaffolds fabricated by concurrent emulsion electrospinning and coaxial cell electrospraying. (A) Morphology and structure of microsphere-embedded scaffolds fabricated via the concurrent manufacturing process. (B) Morphology and structure of 3D cell-incorporated scaffolds fabricated by concurrent manufacturing and subsequent cell release treatment. (C) Comparation of ultimate tensile strength among normal PLGA scaffolds, microsphere-embedded scaffolds and 3D cell-incorporated scaffolds. (D) Comparation of fracture strain among normal PLGA scaffolds, microsphere-embedded scaffolds and 3D cell-incorporated scaffolds. (E) Core-shell meso-structures of emulsion electrospun PLGA nanofibers. (F) In vitro cumulative release profile of VEGF from emulsion electrospun PLGA scaffolds.

of 3D incorporated endothelial cells could be maintained and enhanced by the biomimetic structural cues as well as biochemical cues offered by the bioactive nanofibrous scaffolds, 3D cell-incorporated scaffolds were cultured for 3 and 5 days and evaluated by immunostaining assays, with these scaffolds being used as control: VEGF-containing 2D cell-incorporated scaffolds formed via post-electrospinning manually cell seeding, and VEGF-free 3D cell-incorporated scaffolds formed via the concurrent manufacturing process. Endothelial cells on/in all three types of scaffolds exhibited similar fibroblastic or stellate shapes (Fig. 6A), revealing sufficient cell spreading in both 2D and 3D conditions. By comparing the cell density among different groups, it could be observed that the proliferation of endothelial cells in VEGF-releasing scaffolds (both 2D cell-incorporated scaffolds and 3D cell-incorporated scaffolds) are superior to cell proliferation in VEGF-free scaffolds (Fig. 6A). The sustained and steady release of VEGF had indeed promoted the proliferation of endothelial cells in either 2D or 3D condition, which could contribute to accelerating the formation of confluent endothelial cell monolayer and facilitate vascularization [32]. In 3D cell-incorporated VEGF-releasing scaffolds, some differences in cytoskeleton development were also observed. Endothelial cells in VEGF-releasing 3D cell-incorporated scaffolds displayed highly stressed bundles of F-actin in the cell periphery, which were only few for endothelial cells on VEFG-releasing 2D cell-incorporated scaffolds and in VEFG-free 3D cell-incorporated scaffolds (Fig. 6A). These results indicated that the combined 3D structural and biological cues could enhance the cytoskeleton development of endothelial cells. In addition, the results of immunochemical staining for CD31 and F-actin of endothelial cells on/in the different scaffolds after 5 days of culture showed that the phenotype of endothelial cells was well maintained in 3D cell-incorporated scaffolds (Fig. 6B). The effects of the released VEGF from the scaffolds on stimulating the spreading and proliferation were supported by observations of better stretched cell geometries and higher cell densities for endothelial cells on/in VEGF-releasing scaffolds as compared to those in VEGF-free 3D cell-incorporated scaffolds (Fig. 6B). It was also important to note that sufficiently expressed cytoskeleton proteins with zigzag patterns at the intercellular interface were present only in VEGF-releasing 3D cell-incorporated scaffolds after 3 and 5 days of culture (Figs. 6A and

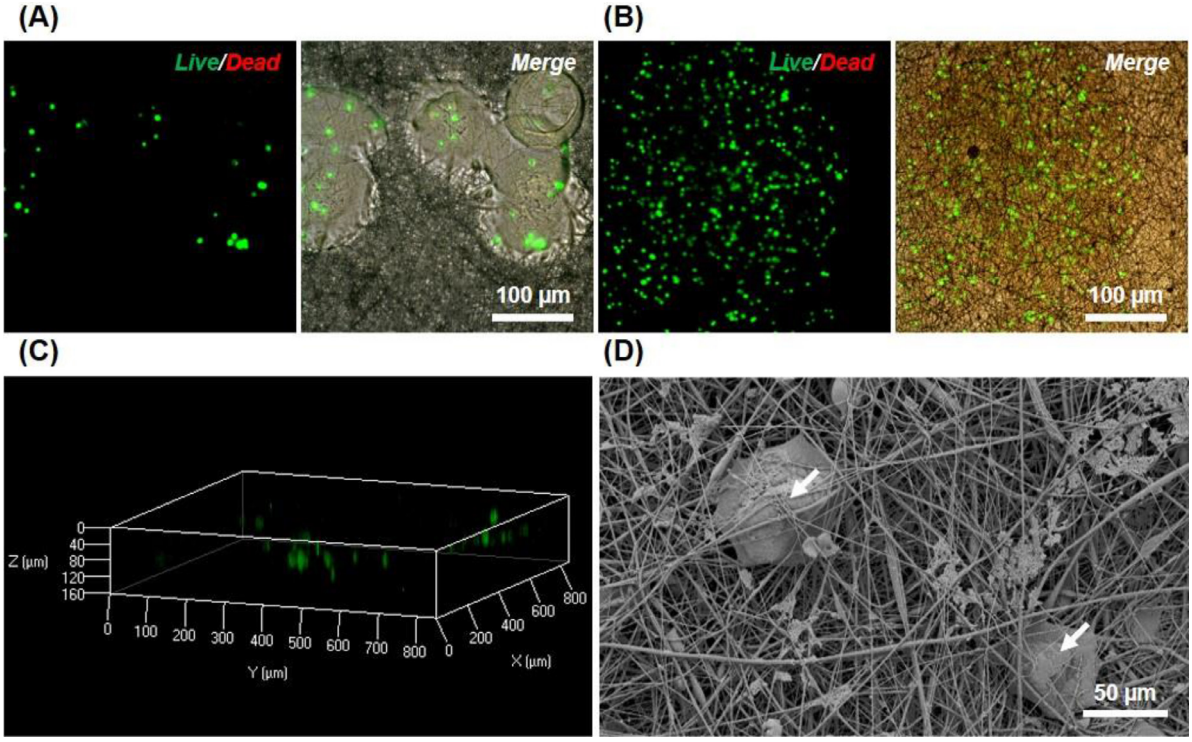

Fig. 5. Viability, distribution, morphology and cytoskeleton development of endothelial cells in bioactive nanofibrous scaffolds fabricated by concurrent emulsion electrospinning and coaxial cell electrospraying. (A) Viability and distribution of HUVECs (stained by using a LIVE/DEAD viability kit) in microsphere-embedded scaffolds with cell staining being performed immediately after the concurrent manufacturing process. (B) Viability and distribution of HUVECs (stained by using a LIVE/DEAD viability kit) in 3D cell-incorporated scaffolds with cell staining being performed immediately after the concurrent manufacturing process and cell release treatment. (C) A representative LSCM image showing the 3D distribution of HUVECs (labelled by Calcein-AM) within 3D cell-incorporated scaffolds after 1-day cell culture. (D) Morphology of 3D cell-incorporated scaffolds after 1-day cell culture, with white arrows indicating well-stretched endothelial cells in the 3D nanofibrous structures.

6B). These results revealed that endothelial cells rapidly formed intercellular connections, which was induced by the biomimetic 3D structural cues and biochemical cues of VEGF-releasing 3D cell-incorporated scaffolds. Since the intercellular connections play vital roles in regulating the integrity of endothelial cell monolayer and the vascular permeability [33,34], it is reasonable to believe that scaffolds fabricated by the concurrent manufacturing process with 3D endothelial cell incorporation, which enable rapid formation of intercellular connections, are very promising to promote 3D vascular remodeling and vascularization.

4. Discussion

Reconstituting 3D cell-laden and vascularized structures to repair body tissues is critical for the success of scaffold-based tissue engineering, which requires effective 3D endothelial cell incorporation and growth. Conventionally, the 3D endothelial cell incorporation within tissue engineering scaffolds relies on cell penetration through interconnected open pores in scaffolds with appropriate pore sizes; and some dynamic cell-seeding methods such as flow perfusion cell seeding or centrifugal force-assisted cell immobilization have been developed for enhancing cell penetration [35,36]. Over the past decade, electrospun scaffolds with ECM-mimicking nanofibrous architectures, adjustable mechanical properties and tailored bioactivity through the controlled release of growth factors have been intensively investigated for tissue engineering. However, there has been the great challenge of 3D cell incorporation within electrospun nanofibrous scaffolds due to their usually very small sizes of interconnected pores, which has greatly limited their applications in the regeneration of thick and vascularized human body tissues. For electrospun nanofibrous scaffolds, even dynamic cell-seeding methods are inadequate for improving cell penetration. Previous studies by many researchers for achieving 3D cell incorporation within electrospun scaffolds therefore focus mainly on developing strategies to enlarge the pore size in scaffolds. Despite some degrees of success in enhancing cell penetration into electrospun scaffolds via enlarged interconnected pores, inherent conflict between deep cell penetration, which requires loose structures, and structural integrity of nanofibrous scaffolds appears insurmountable, which greatly limits the potential of electrospun scaffolds for engineering 3D cellularized constructs or regenerating complex body tissues/organs. In contrast, through concurrent emulsion electrospinning and coaxial cell electrospraying, cells in hydrogel microspheres are co-deposited with electrospun nanofibers and therefore placed directly within the nanofibrous architectures of the scaffolds formed, rather than being incorporated via a post-electrospinning cell seeding process. Our results have shown that the incorporated cells maintained high viability, spread and proliferated well, and showed enhanced cytoskeleton development and phenotype owing to the 3D environment for cells. Therefore, our concurrent manufacturing technology has successfully addressed the challenge of enabling deep 3D cell incorporation and maintaining structural integrity for electrospun scaffolds as cell incorporation does not depend on cell penetration into loose and hence weakened scaffolds.

Using the concurrent emulsion electrospinning and coaxial cell electrospraying process, vascular endothelial cells are firstly encapsulated in Ca-alginate hydrogel microspheres. Due to the mild condition to crosslink Na-alginate and good cytocompatibility of crosslinked Ca-alginate hydrogel [26], the encapsulated vascular endothelial cells show well-preserved cell viability (>98%). In addition, as reported by others, Ca-alginate hydrogel is superior in molecular diffusion and mass exchange [37], which is important for maintaining the metabolism and long-term survival of encap-

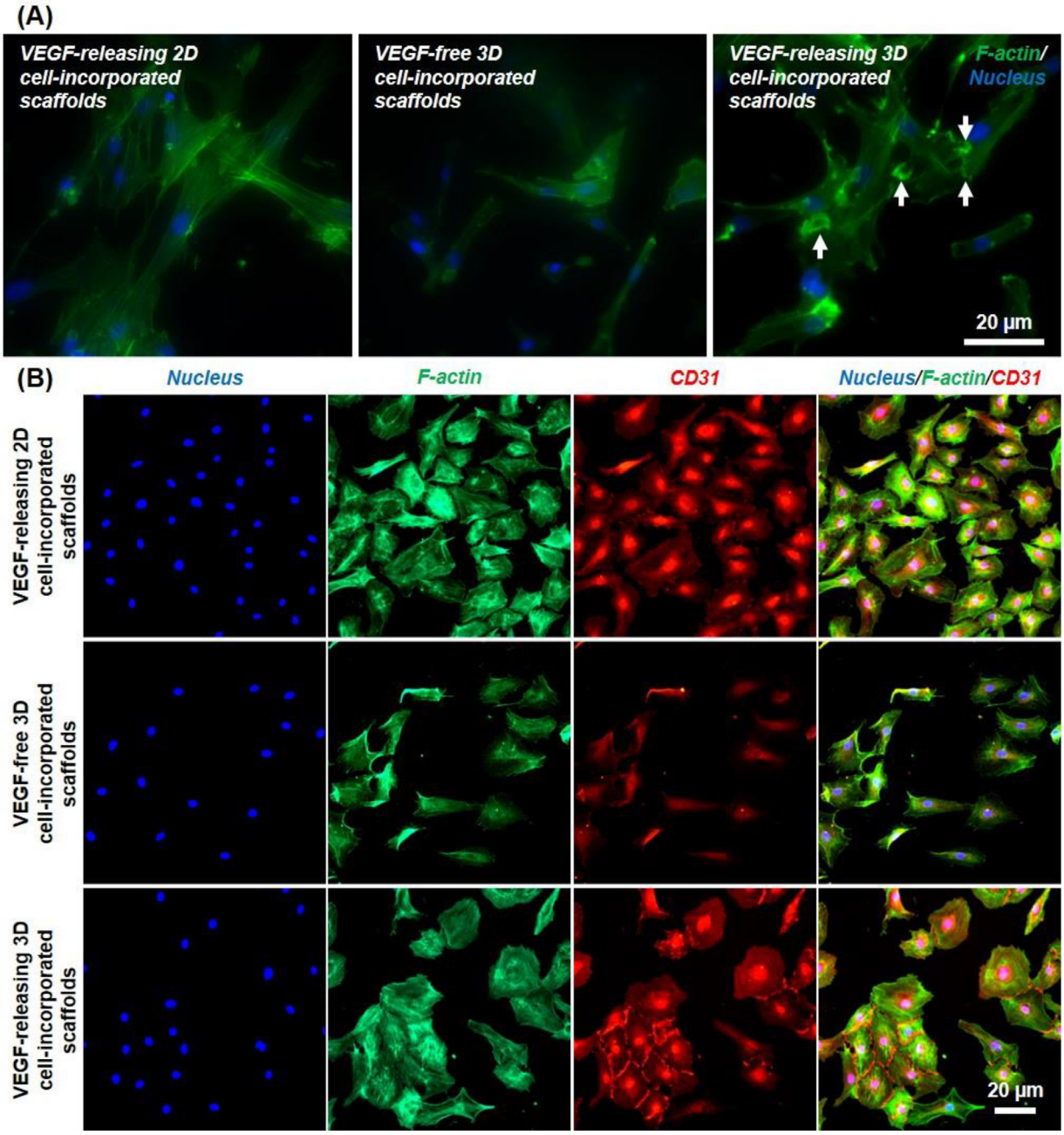

Fig. 6. Cytoskeleton development and phenotypes of endothelial cells cultured on or in VEGF-releasing 2D cell-incorporated, VEGF-free 3D cell-incorporated and VEGF-releasing 3D cell-incorporated scaffolds. (A) Cytoskeleton development of endothelial cells grown on or in the nanofibrous scaffolds (either VEGF-free or VEGF-releasing) after 3-day cell culture, with the white arrows indicating the intercellular connections formed. (B) Morphology and phenotypes of endothelial cells grown on or in the nanofibrous scaffolds (either VEGF-free or VEGF-releasing) after 5-day cell culture.

sulated cells. Furthermore, it is shown that the crosslinked Ca-alginate hydrogel microspheres can be broken down by the Na-citrate solution treatment, which is due to the high affinity between alginate and citrate [26], making it possible for the encapsulated cells to be released on demand. Thanks to the effective protection by and on-demand release of cells from electrosprayed Ca-alginate microspheres, 3D endothelial cell incorporation and high structural integrity of scaffolds have been simultaneously achieved by using the concurrent manufacturing approach for scaffold construction. In addition, with the provision of biomimetic structural cues and biological cues, the functions and phenotype of endothelial cells can be effectively maintained and promoted in 3D cell-incorporated scaffolds formed by the concurrent manufacturing process. Even though the enzymes and cations for breaking down Ca-alginate hydrogel are not present in human bodies, 3D cell-incorporated scaffolds that resemble the native 3D cell-laden and vascularized structures of body tissues can be formed prior to *in vivo* implantation by releasing the encapsulated cells *in vitro* via the Na-citrate solution treatment. Therefore, the 3D cell-incorporated scaffolds with tissue-mimicking 3D cell-nanofiber organizations holds great promise for the regeneration of complex body tissues/organs. They may also be very useful for the building of tissue/disease models for *in vitro* drug screening.

To reconstitute or replicate the complex anatomy and functions of human body tissues with well-defined multicellular organizations is a highly challenging goal in tissue engineering but must

be properly and well addressed [38]. Apart from our concurrent emulsion electrospinning and coaxial cell electrospraying technique, bioprinting is a popular approach for biomanufacturing 3D cell-incorporated structures, particularly those with well-defined multicellular organizations, e.g., vascularized cell-laden structures [39–41]. However, bioprinted structures face a common problem that the cells are usually encapsulated within hydrogel structs, resulting in sometimes confined cell spreading, limited intercellular interactions and slow tissue remodeling. With appropriate architecture, mechanical properties and bioactivity, electrospun nanofibrous scaffolds have shown advantages in supporting cell spreading, promoting intercellular interactions, and potentially enhancing tissue remodeling [6]. So far, the incorporation of different types of cells within electrospun scaffolds in specific positions to form 3D cell-incorporated structures with well-defined multicellular organizations has not been addressed. Existing methods to control the distributions of different types of cells within cell-laden electrospun scaffolds are usually to separately seed different types of cells onto the two different surfaces of scaffolds [42], resulting in short depth in cell penetration and limited patterns in the spatial organizations of different cells. Our concurrent emulsion electrospinning and coaxial cell electrospraying technology provides a promising alternative for biomanufacturing 3D cell-incorporated structures with well-defined multicellular organizations as the spatial layout/organizations of cells can be controlled for nanofibrous scaffolds during the concurrent manufacturing process. In addition, compared to bioprinted structures, 3D cell-incorporated structures formed by the concurrent manufacturing technology can potentially achieve better cell spreading and intercellular connections for the incorporated cells that are supported by the nanofibrous scaffolds with interconnected pores and spatiotemporally controlled release of growth factors, making technology potentially very useful for stem cell engineering and organoid 3D culture [43]. In our current proof-of-concept investigations, the depth of cell distribution through the scaffold thickness is just about 100 μm and only one type of cell, the endothelial cell, is incorporated. With the high versatility and expansibility of our concurrent manufacturing technology, it should be feasible to extend this technology to construct 3D cell-incorporated nanofibrous structures with a large thickness and with well-defined multicellular organizations by simply prolonging the co-deposition time and by sequentially performing coaxial cell electrospraying with the use of different types of cells. For producing such structures, it is extremely difficult, if possible, for the existing scaffold-based tissue engineering strategies that rely on cell penetration. On the other hand, to successfully make 3D cell-incorporated structures with well-defined multicellular organizations by employing our concurrent manufacturing technology, we shall need to address the technical challenge of precisely controlling the spatial distributions of different cell types. The integration of an advanced bioprinting technology with our concurrent manufacturing technology should be investigated to deal with this challenge. Also, the issue of immunogenicity of incorporated cells must be carefully considered in the future work of *in vivo* studies of 3D cell-incorporated structures. Regarding immunogenicity, 3D cell-incorporated structures can be built by harvesting autologous cells for cell incorporation as one possible solution [44]. The 3D cell-incorporated structures resembling the complex anatomies of native body tissues/organs are also potentially very useful for regenerating the body tissues/organs in which constituting cells lack the renewal capability [45,46].

5. Conclusion

Concurrent emulsion electrospinning and coaxial cell electrospraying is established for the effective fabrication of 3D cell-incorporated nanofibrous tissue engineering scaffolds. In this proof-of-concept study, 3D endothelial cell-incorporated and VEGF-incapsulated nanofibrous scaffolds are successfully made via the concurrent manufacturing process. Through coaxial cell electrospraying, endothelial cells are encapsulated in Ca-alginate hydrogel microspheres during scaffold fabrication and can be released on demand subsequently. The viability of the cells is well preserved during the scaffold manufacture and cell release processes. Emulsion electrospinning enables the production of bioactive nanofibrous scaffolds, with VEGF being protected and encapsulated in the aqueous cores of electrospun nanofibers, and VEGF can be released from the fibers in a sustained and steady manner. By integrating coaxial cell electrospraying with emulsion electrospinning, living endothelial cells can be placed randomly within VEGF-releasing nanofibrous scaffolds. The endothelial cells incorporated in 3D in nanofibrous scaffolds can stretch sufficiently in 3D, proliferate well, maintain the phenotype, and rapidly form intercellular connections owing to the combined biomimetic structural and biochemical cues. Our concurrent manufacturing technology not only offers an effective approach to solve the inherent problem of 3D deep cell incorporation within electrospun nanofibrous scaffolds but also provides a promising biomanufacturing platform for reconstituting 3D cell-ECM organizations *in vitro*, which will enable significant advances in the engineering of complex tissue-like 3D cell-incorporated constructs for tissue engineering, drug screening, and other biomedical applications.

Declaration of Competing Interest

There are no conflicts of interest to declare.

Acknowledgements

This work was supported by the National Key R&D Program of China (2017YFA0701303), the National Natural Science Foundation of China (51903245), Hong Kong Research Grants Council (HKU 7177/13E, 17201017), and the Fundamental Research Program of Shenzhen (JCYJ20170818161757684, JCYJ20170307164610282).

Supplementary materials

Supplementary material associated with this article can be found, in the online version, at doi:10.1016/j.actbio.2021.01.035.

References

[1] L.L. Hench, J.M. Polak, Third-generation biomedical materials, Science 295 (2002) 1014–1017.
[2] R.O. Hynes, The extracellular matrix: not just pretty fibrils, Science 326 (2009) 1216–1219.
[3] G. Huang, F. Li, X. Zhao, Y. Ma, Y. Li, M. Lin, G. Jin, T.J. Lu, G.M. Genin, F. Xu, Functional and biomimetic materials for engineering of the three-dimensional cell microenvironment, Chem. Rev 117 (2017) 12764–12850.
[4] E.S. Place, N.D. Evans, M.M. Stevens, Complexity in biomaterials for tissue engineering, Nat. Mater. 8 (2009) 457–470.
[5] M.P. Lutolf, J.A. Hubbell, Synthetic biomaterials as instructive extracellular microenvironments for morphogenesis in tissue engineering, Nat. Biotechnol. 23 (2005) 47–55.
[6] Q. Zhao, H. Cui, J. Wang, H. Chen, Y. Wang, L. Zhang, X. Du, M. Wang, Regulation effects of biomimetic hybrid scaffolds on vascular endothelium remodeling, ACS Appl. Mater. Interfaces 10 (2018) 23583–23594.
[7] K.S. Ogueri, C.T. Laurencin, Nanofiber technology for regenerative engineering, ACS Nano 14 (2020) 9347–9363.
[8] J. Ding, J. Zhang, J. Li, D. Li, C. Xiao, H. Xiao, H. Yang, X. Zhuang, X. Chen, Electrospun polymer biomaterials, Prog. Polym. Sci 90 (2019) 1–34.
[9] S. Khorshidi, A. Solouk, H. Mirzadeh, S. Mazinani, J.M. Lagaron, S. Sharifi, S. Ramakrishna, A review of key challenges of electrospun scaffolds for tissue-engineering applications, J. Tissue Eng. Regen. Med 10 (2016) 715–738.
[10] S. Zhong, Y. Zhang, C.T. Lim, Fabrication of large pores in electrospun nanofibrous scaffolds for cellular infiltration: a review, Tissue Eng. Pt. B 18 (2012) 77–87.
[11] M.C. Phipps, W.C. Clem, J.M. Grunda, G.A. Clines, S.L. Bellis, Increasing the pore sizes of bone-mimetic electrospun scaffolds comprised of polycaprolactone, collagen I and hydroxyapatite to enhance cell infiltration, Biomaterials 33 (2012) 524–534.

[12] C. Vaquette, J.J. Cooper-White, Increasing electrospun scaffold pore size with tailored collectors for improved cell penetration, Acta Biomater. 7 (2011) 2544–2557.
[13] J. Rnjak-Kovacina, A.S. Weiss, Increasing the pore size of electrospun scaffolds, Tissue Eng. Pt. B 17 (2011) 365–372.
[14] B.A. Blakeney, A. Tambralli, J.M. Anderson, A. Andukuri, D.J. Lim, D.R. Dean, H.W. Jun, Cell infiltration and growth in a low density, uncompressed three-dimensional electrospun nanofibrous scaffold, Biomaterials 32 (2011) 1583–1590.
[15] B.M. Baker, A.O. Gee, R.B. Metter, A.S. Nathan, R.A. Marklein, J.A. Burdick, R.L. Mauck, The potential to improve cell infiltration in composite fiber-aligned electrospun scaffolds by the selective removal of sacrificial fibers, Biomaterials 29 (2008) 2348–2358.
[16] J.J. Stankus, J. Guan, K. Fujimoto, W.R. Wagner, Microintegrating smooth muscle cells into a biodegradable, elastomeric fiber matrix, Biomaterials 27 (2006) 735–744.
[17] X.C. Yang, J.D. Shah, H.J. Wang, Nanofiber enabled layer-by-layer approach toward three-dimensional tissue formation, Tissue Eng. Pt. A 15 (2009) 945–956.
[18] Q. Zhao, H. Cui, Y. Wang, X. Du, Microfluidic Platforms toward rational material fabrication for biomedical applications, Small 16 (2019) 1903798.
[19] M.A. Bochenek, O. Veiseh, A.J. Vegas, J.J. McGarrigle, M. Qi, E. Marchese, M. Omami, J.C. Doloff, J. Mendoza-Elias, M. Nourmohammadzadeh, A. Khan, C.-.C. Yeh, Y. Xing, D. Isa, S. Ghani, J. Li, C. Landry, A.R. Bader, K. Olejnik, M. Chen, J. Hollister-Lock, Y. Wang, D.L. Greiner, G.C. Weir, B.L. Strand, A.M.A. Rokstad, I. Lacik, R. Langer, D.G. Anderson, J. Oberholzer, Alginate encapsulation as long-term immune protection of allogeneic pancreatic islet cells transplanted into the omental bursa of macaques, Nat. Biomed. Eng. 2 (2018) 810–821.
[20] H. Ye, K. Zhang, D. Kai, Z. Li, X.J. Loh, Polyester elastomers for soft tissue engineering, Chem. Soc. Rev. 47 (2018) 4545–4580.
[21] Q. Zhao, W.W. Lu, M. Wang, Modulating the release of vascular endothelial growth factor by negative-voltage emulsion electrospinning for improved vascular regeneration, Mater. Lett. 193 (2017) 1–4.
[22] Q. Zhao, M. Wang, Manipulating the release of growth factors from biodegradable microspheres for potentially different therapeutic effects by using two different electrospray techniques for microsphere fabrication, Polym. Degrad. Stabil. 162 (2019) 169–179.
[23] S.N. Jayasinghe, J. Auguste, C.J. Scotton, Platform technologies for directly reconstructing 3d living biomaterials, Adv. Mater. 27 (2015) 7794–7799.
[24] P. Davoodi, F. Feng, Q. Xu, W.C. Yan, Y.W. Tong, M.P. Srinivasan, V.K. Sharma, C.H. Wang, Coaxial electrohydrodynamic atomization: microparticles for drug delivery applications, J. Control. Release 205 (2015) 70–82.
[25] N. Bock, T.R. Dargaville, M.A. Woodruff, Electrospraying of polymers with therapeutic molecules: state of the art, Prog. Polym. Sci. 37 (2012) 1510–1551.
[26] J. Jia, D.J. Richards, S. Pollard, Y. Tan, J. Rodriguez, R.P. Visconti, T.C. Trusk, M.J. Yost, H. Yao, R.R. Markwald, Y. Mei, Engineering alginate as bioink for bioprinting, Acta Biomater. 10 (2014) 4323–4331.
[27] G.S. Hussey, J.L. Dziki, S.F. Badylak, Extracellular matrix-based materials for regenerative medicine, Nat. Rev. Mater. 3 (2018) 159–173.
[28] J.M. Bourget, R. Gauvin, D. Larouche, A. Lavoie, R. Labbe, F.A. Auger, L. Germain, Human fibroblast-derived ECM as a scaffold for vascular tissue engineering, Biomaterials 33 (2012) 9205–9213.
[29] L.M.C. Aguilar, S.M. Silva, S.E. Moulton, Growth factor delivery: defining the next generation platforms for tissue engineering, J. Control. Release 306 (2019) 40–58.
[30] Q. Zhao, J. Wang, H. Cui, H. Chen, Y. Wang, X. Du, Programmed shape-morphing scaffolds enabling facile 3d endothelialization, Adv. Funct. Mater. 28 (2018) 1801027.
[31] M.M. Stevens, J.H. George, Exploring and engineering the cell surface interface, Science 310 (2005) 1135–1138.
[32] R.C.A. Eguiluz, K.B. Kaylan, G.H. Underhill, D.E. Leckband, Substrate stiffness and VE-cadherin mechano-transduction coordinate to regulate endothelial monolayer integrity, Biomaterials 140 (2017) 45–57.
[33] E. Dejana, Endothelial cell-cell junctions: happy together, Nat. Rev. Mol. Cell Biol. 5 (2004) 261–270.
[34] Q. Zhao, J. Wang, Y. Wang, H. Cui, X. Du, A stage-specific cell-manipulation platform for inducing endothelialization on demand, Natl. Sci. Rev. 7 (2020) 629–643.
[35] F.P. Melchels, B. Tonnarelli, A.L. Olivares, I. Martin, D. Lacroix, J. Feijen, D.J. Wendt, D.W. Grijpma, The influence of the scaffold design on the distribution of adhering cells after perfusion cell seeding, Biomaterials 32 (2011) 2878–2884.
[36] T.H. Yang, H. Miyoshi, N. Ohshima, Novel cell immobilization method utilizing centrifugal force to achieve high-density hepatocyte culture in porous scaffold, J. Biomed. Mater. Res. 55 (2001) 379–386.
[37] J.M.C. Puguan, X. Yu, H. Kim, Diffusion characteristics of different molecular weight solutes in Ca-alginate gel beads, Colloids Surf., A 469 (2015) 158–165.
[38] S.V. Murphy, A. Atala, Organ engineering–combining stem cells, biomaterials, and bioreactors to produce bioengineered organs for transplantation, BioEssays 35 (2013) 163–172.
[39] D.B. Kolesky, K.A. Homan, M.A. Skylar-Scott, J.A. Lewis, Three-dimensional bioprinting of thick vascularized tissues, Proc. Natl. Acad. Sci. USA 113 (2016) 3179–3184.
[40] H.W. Kang, S.J. Lee, I.K. Ko, C. Kengla, J.J. Yoo, A. Atala, A 3D bioprinting system to produce human-scale tissue constructs with structural integrity, Nat. Biotechnol. 34 (2016) 312–319.
[41] S.V. Murphy, A. Atala, 3D bioprinting of tissues and organs, Nat. Biotechnol. 32 (2014) 773–785.
[42] X. Dong, X. Yuan, L. Wang, J. Liu, A.C. Midgley, Z. Wang, K. Wang, J. Liu, M. Zhu, D. Kong, Construction of a bilayered vascular graft with smooth internal surface for improved hemocompatibility and endothelial cell monolayer formation, Biomaterials 181 (2018) 1–14.
[43] J.A. Brassard, M.P. Lutolf, Engineering stem cell self-organization to build better organoids, Cell Stem Cell 24 (2019) 860–876.
[44] L.S. Saleh, S.J. Bryant, The host response in tissue engineering: crosstalk between immune cells and cell-laden scaffolds, Curr. Opin. Biomed. Eng. 6 (2018) 58–65.
[45] J. Yang, Y.S. Zhang, K. Yue, A. Khademhosseini, Cell-laden hydrogels for osteochondral and cartilage tissue engineering, Acta Biomater. 57 (2017) 1–25.
[46] M. Montgomery, S. Ahadian, L.D. Huyer, M.L. Rito, R.A. Civitarese, R.D. Vanderlaan, J. Wu, L.A. Reis, A. Momen, S. Akbari, A. Pahnke, Flexible shape-memory scaffold for minimally invasive delivery of functional tissues, Nat. Mater. 16 (2017) 1038–1046.